Technical Design Report

James Madison University Prototype Development Sub-Team's Report
Submitted to the 2021 Collegiate Wind Competition Organizers
at the U.S. Department of Energy
on May 23rd, 2021
in fulfillment of the requirements for the Technical Design Report submission

by

Nikola Bajs- Secondary Lead Coding

Raymond Benner- Primary Lead Generator

Tre Bright- Primary Lead Mechanical Design

George Funk- Secondary Lead Mechanical Design

Brady Monroe- Primary Lead Blades

Nathaniel Ray- Primary Lead Coding

Leith Rayes- Secondary Lead Blades

Jaclyn Riddiford- Primary Lead Controls

Faculty Advisors

Dr. Stephen K. Holland, Ph.D.
Dr. Jonathon Miles, Ph.D.
Mr. Edwin Clamp

Table of Contents

Executive Summary

The JMU team emphasized simplicity of fabrication and assembly for the 2021 prototype design competition. The university's COVID-19 pandemic response resulted in significant uncertainty about access to laboratory and fabrication studios, purchasing, and materials acquisition. Due to the interruption of the 2020 CWC, an existing turbine prototype was not available to the 2021 team to reference. Therefore, emphasis was placed on design for fabrication, assembly, and testing to ensure completion of a functional turbine to meet competition objectives. While various design concepts were considered, a three-blade, fixed pitch, horizontal axis rotor with a passive yaw system was ultimately selected. Blades, 3D printed from Onyx material, were designed for a tip-speed ratio of 3.0 using the Wortmann FX 60-126 root and the SG6043 tip airfoil profiles. Electrical power is produced by a team-designed direct drive, axial flux, three-phase permanent magnet generator composed of two rotors, each with 12 neodymium magnets, and a 9-coil stator. The hand wound stator coils, each with 225 turns of 28 gage magnet wire, were designed to match required generator torque with simulated blade rotor torque and rotational speed characteristics to maximize power power production. A digitally controlled current sink into a load resistor serves as the turbine load.

For turbine safety and control of rated power tasks, an Actuonix PQ12 linear servo is used to actuate a cable driven disc brake mounted inside the turbine nacelle. When the turbine is in a state of emergency, such as when power is lost or the emergency stop button is pressed, the brake system brings the turbine rotors to a complete stop. The brake system is also designed to engage and disengage the brake rotor to maintain steady power output during higher wind speed conditions.

Many changes were made to the turbine's electrical system from the JMU 2020 team design. Custom printed circuit boards are used for the turbine's electrical system for connection reliability and easier troubleshooting. The three phase AC generated power is rectified, regulated to a constant voltage and distributed throughout the system to an actuator, sensors, microcontroller, the PCC, and load using commercially available connectors and wires. The turbie side and load side electronics are housed separately in NEMA 1 rated enclosures.

The turbine is controlled by two Arduinos, one in the load NEMA enclosure and the other in the turbine NEMA enclosure. The load Arduino is the primary controller and control states are based on RPM readings from the optical encoder mounted on the turbine driveshaft. The controllers monitor generator power, current and voltage along with the output power, current and voltage. They also monitor the emergency stop condition, brake condition and load settings.

This report details the JMU 2021 CWC team's prototype design process, design decisions, control scheme, testing results, and recommendations for future teams. Due to planning and design for manufacturing, a fully functional turbine was fabricated and demonstrated at JMU. Testing results indicated that the balanced design objectives were achieved, attaining a cut-in wind speed of 3.7 m/s, a power output of 22.2 W at 9 m/s wind speeds, stable yaw, and effective maximum power point tracking control. The turbine was able to successfully shutdown and immediately restart after the E-stop switch and load disconnect safety conditions were initiated. The turbine was demonstrated to maintain a steady 17 W output and relatively constant rotational speed at wind conditions between 8.5 m/s and 9 m/s through modulation of the disk brake clamping force.

Along with successfully designing, fabricating, and testing a prototype turbine to achieve the tasks listed in the 2021 Rules and Requirements, the team hopes to provide future CWC teams with useful information that can impact their design process. Therefore, this design report will not only detail JMU's 2021 turbine prototype, but also provide recommendations for future teams benchmarking this year's turbine design.

1. Blade Design

1.1 Design Considerations

The JMU 2020 competition team performed an extensive analysis of airfoils, which were used as the basis for the 2021 team's blade design study. The team also benchmarked past competition teams' designs in order to arrive at a narrow list of candidate airfoils. Due to the size of the prototype turbine, airfoil profiles having high lift to drag ratios (c_l/c_d) at low Reynolds numbers (40,000 - 50,000) were modeled. The Wortmann FX 60-126 and SG6043 emerged as the two primary airfoil candidates due to high c_l/c_d and large peak lift coefficients at an angle of attack of approximately 8° as shown in Figure 1.

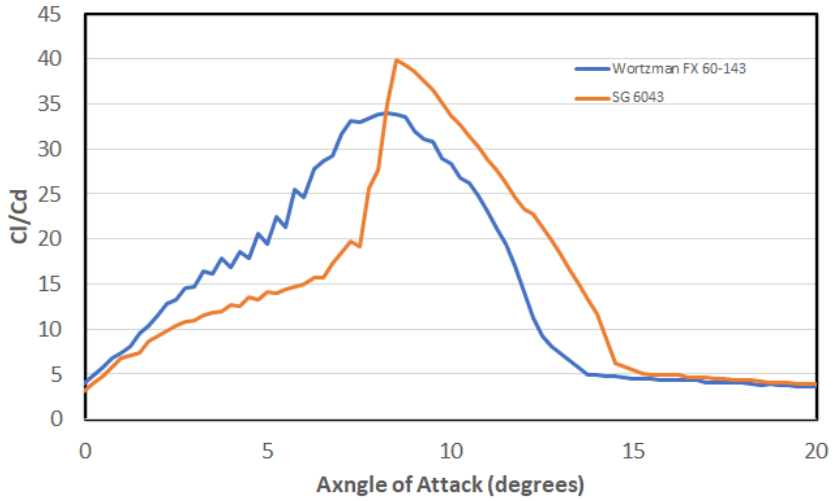

***Figure 1**: L/D Ratio vs. Angle of Attack*

The Blade Element Momentum (BEM) theory simulations were performed using QBlade[1] to design and optimize the rotor. These simulation results were then further examined by exporting power production, torque, and rotational speed simulations into Excel and Matlab models. The JMU team's Excel spreadsheets and Matlab code allows for comparison of simulated rotor parameters with those of an axial flux generator. Turbine rotor blades must be designed for compatibility with the generator, ensuring adequate torque production and operational speeds for the desired voltage and power outputs. These simulations allowed the team to rapidly simulate this compatibility when considering blades designed with different airfoils and tip-speed ratios.

While the 2020 competition team opted for a single airfoil blade profile using the FX 60-126, the 2021 team recognized the enhanced lift-to-drag performance of the SG6043. However, the FX60-126 airfoil has greater thickness (12.5% chord) than the SG6043 (10% chord) with the potential for greater structural integrity. As a result, the team opted for a combination blade design using the FX 60-126 as the root profile and the SG6043 as the tip profile.

Due to the inclusion of a high voltage input buck-boost converter and the recognition that higher tip-speed ratio blade designs result in higher coefficients of performance (C_p), the 2021 team sought to increase the operating tip speed ratio (TSR) of prior teams' designs. However, the increased tip speed ratio design needed to be balanced with the starting torque required for low-wind speed cut-in. Since the team opted for a fixed-pitch blade design for fabrication and assembly simplification, the rotor blades must be capable of producing sufficient torque to overcome the drivetrain friction at low wind speeds. Following simulation and evaluation of competition scoring potential from numerous designs, conducted with QBlade the JMU developed generator simulation code, a blade design optimized for a TSR of 3.0 was identified as providing the desired balance between cut-in performance and power production.

The final rotor design is a three blade, fixed pitch, 18 cm blade attached to a 4 cm hub. The blade's twist and chord profile was optimized for TSR of 3.0 using Schmitz optimization [1]. A detailed

table of the blade's characteristics at each section along its blade span is provided in Table 1. BEM simulations predict a coefficient of performance, C_p, of 0.375 (37.5%) when operating at the design TSR, as illustrated by simulation results presented in Figure 2.

***Table 1**: Final Blade Design Characteristics*

Station Number	Radial Position [m]	Chord Length [cm]	Twist [deg]	Airfoil Name
1.00	2.50E-02	1.00	0.00	Circular Foil
2.00	3.50E-02	1.00	0.00	Circular Foil
3.00	4.50E-02	1.00	0.00	Circular Foil
4.00	5.50E-02	6.86	34.02	FX 60-123
5.00	6.50E-02	6.80	29.32	FX 60-123
6.00	7.50E-02	6.62	25.44	FX 60-123
7.00	8.50E-02	6.38	22.22	FX 60-123
8.00	9.50E-02	6.11	19.51	FX 60-123
9.00	1.05E-01	5.18	16.96	SG 6043
10.00	1.15E-01	4.93	15.00	SG 6043
11.00	1.25E-01	4.70	13.30	SG 6043
12.00	1.35E-01	4.47	11.82	SG 6043
13.00	1.45E-01	4.26	10.53	SG 6043
14.00	1.55E-01	4.06	9.38	SG 6043
15.00	1.65E-01	3.88	8.36	SG 6043
16.00	1.75E-01	3.71	7.45	SG 6043
17.00	1.85E-01	3.55	6.62	SG 6043
18.00	1.95E-01	3.40	5.88	SG 6043
19.00	2.05E-01	3.26	5.21	SG 6043
20.00	2.15E-01	3.14	4.59	SG 6043
21.00	2.25E-01	3.02	4.03	SG 6043

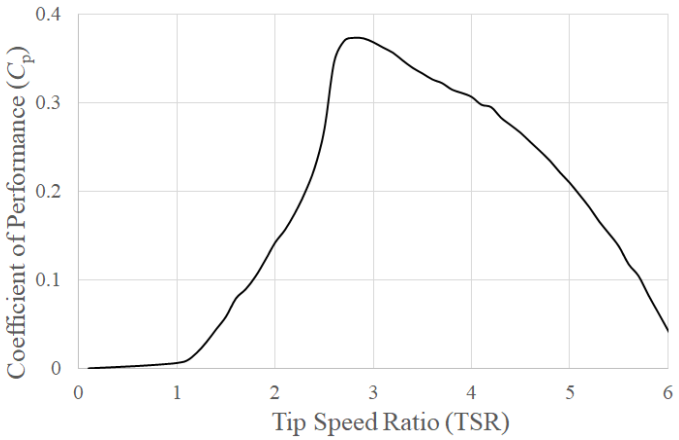

***Figure 2**: Coefficient of Performance vs. TSR*

1.2 Fabrication

The turbine blades and hub were 3D printed in JMU Department of Engineering's fabrication studio. Although different fabrication methods were considered, 3D printing was deemed the most cost and time effective given pandemic response limitations. The selected QBlade derived design was converted into a SolidWorks model, where hub connection points were added. The first iteration of

turbine blades were printed using ABS filament. The fixed-pitch blades were affixed to the hub, designed with three extrusions into which each blade was mounted and secured with two 5-40 machine screws, as shown in Figures 3 and 4. A second iteration of blades were printed using Onyx thermoplastic filament, a nylon and carbon fiber composite [2]. Subsequent tests were performed to determine which set of blades to include in the final prototype.

***Figure 3**: Turbine Blade and Hub Design*

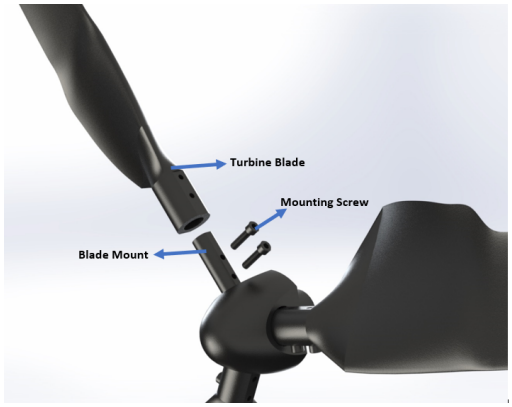

***Figure 4**: Blade Mounting Exploded View*

1.3 Stress Analysis and Material Selection

The base of the turbine blades and connection points to the hub must withstand both radial forces, due to high rotational speeds, and axial forces, associated with the incoming wind. Simulation testing was conducted in QBlade to estimate the expected loads on the blades under operational conditions for both 11 m/s and as well 22 m/s. These simulated loadings were then used as input to a SolidWorks simulation study to identify the weakest points along the blade and hub. Two 3D printed materials, ABS and Onyx, were considered for blade and hub manufacturing, with final selection being based upon simulations and physical testing. Ultimately, Onyx was chosen due to its lightweight , flexible, and high yield strength material properties. Each blade weighs roughly 0.36 newtons with a yield strength of 48 MN/m^2.

With expected rotational speeds above 2000 RPM, radial forces represent the most significant load, estimated to be approximately 122 N on each blade. With this radial loading, a safety factor of 3.4 was estimated for blades fabricated using the Onyx filament. Simulation testing showed that both loading and centrifugal force placed the most amount of stress on the same location near the root mounting holes, as illustrated in Figures 5 (axial loading) and 6 (radial loading). Physical static load tests were also performed on the blade, hub, turbine tower, and nacelle to verify the results provided by SolidWorks simulation.

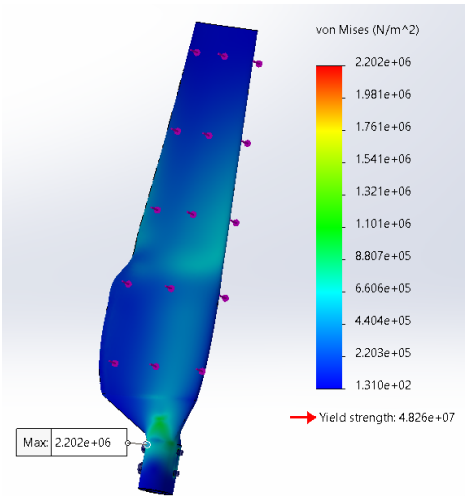

***Figure 5**: Onyx Axial Load Stress Plot*

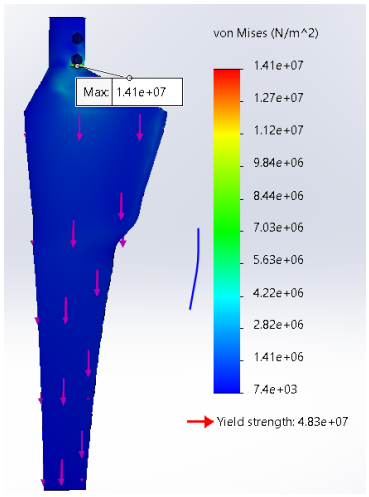

***Figure 6**: Onyx Radial Load Stress Plot*

Axial load deflection tests were carried out for the two candidate blade materials with loads applied at the center of mass A dial indicator was mounted under the blade to measure deflection as weight was incrementally added, as shown in Figure 7. Each blade was tested until failure to compare with simulation results. Figure 8 shows the fracture point of the ABS blade when 49 N was applied. Physical testing confirmed simulation results. The Onyx blade however, did not break; rather, it deflected a significant amount, resulting in deformation. Failure for the Onyx blade was thus defined as the deflection distance at which the blade could potentially strike the turbine tower, or approximately 0.13 meters. Test results for each blade were documented and are compared in Table 2.

***Figure 7**: Onyx Blade Axial Deflection Test*

***Figure 8**: Static Axial Load Fracture Point*

***Table 2**: Turbine Blade Material Axial Loading Test Results*

ABS			Onyx		
Applied Load(N)	Deflection(in)	*Factor of Safety(Load)	Applied Load(N)	Deflection(in)	*Factor of Safety(Load)
11.1	.005	**20**	11	0.34	**22**
22.2	**.**181		22.2	0.73	
33.4	0.23		33.4	1.35	

**Onyx blade failure is the point at which the blade makes contact with turbine tower ~ 5 inches*
**ABS blade failure is the point at which the blade breaks or fractures*

2. Mechanical and Structural Design

The structural components of the turbine include the nacelle, tower, and baseplate. The nacelle houses and supports the direct drive drivetrain, axial flux generator, and a cable driven disc brake. The nacelle is mounted to the tower and aligned upwind using a passive yaw bearing configuration and tail-fin mounted to the nacelle. The mechanical system design emphasizes simplicity for fabrication and assembly while meeting the requirements for the CWC's safety, durability, and performance tasks.

The turbine's nacelle, brake rotor, baseplate, and as well tower were fabricated from 6061 aluminum due to its non magnetic and light-weight material properties. Each nacelle plate was manufactured using a Haas 3-axis CNC machine, whereas a lathe and mill machine were key resources for machining the brake rotor and turbine baseplate.

2.1 Nacelle Design

The turbine's nacelle design provides structure for mounting the driveshaft, generator, brake system, optical encoder, and as well AC to DC rectifier, as shown in Figure 9. The objective was to maintain simplicity throughout the design by only mounting components inside the nacelle that rely on the rotation of the driveshaft, excluding the rectifier. To ensure the design had proper fitment to satisfy the 45cm x 45cm x 45cm size requirement, SolidWorks CAD assembly models were created prior to fabrication. The nacelle structure is machined from 6061 aluminum, and fastened by 5-40 hex head machine screws. The driveshaft is machined with a d-shape profile to reduce slip of components mounted to the driveshaft. Two ball bearings are press-fit into the front and rear nacelle plates to support the driveshaft and lock collars are positioned on each end of the driveshaft to secure it in place.

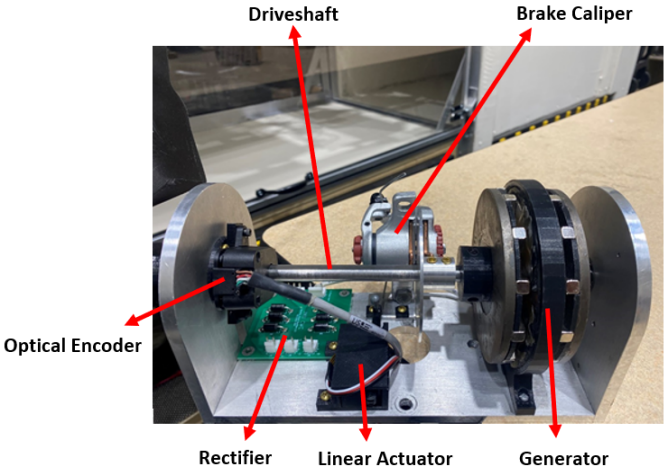

***Figure 9**: Nacelle Design*

The blade rotor hub and generator rotors were 3D printed from ABS plastic and are secured to the driveshaft with two set screws each. Aluminum thread-to-expand inserts were incorporated into the 3D printed plastic parts to allow the set screws to firmly seat against the driveshaft, as shown below in Figure 10. This prevents the use of plastic threads that can easily strip, a problem encountered with prior competition teams' designs.

The turbine's braking system is a cable driven brake caliper with an aluminum brake rotor mounted to the driveshaft. The cable is connected to an Actuonix PQ12 linear servo that is controlled by the turbine side Arduino microcontroller. The linear actuator has a 100:1 gear ratio and 50 N drive force. The increased gear ratio sacrifices actuator speed for increased clamping force to ensure the brake caliper can bring the brake rotor to a stop. The gearing configuration of the actuator allows it to hold the last commanded servo position even when power is removed. By maintaining clamping force, the PQ12 linear actuator allows the rotor to remain in a parked state when power is unavailable from the generator or the load. Each component for the brake design is displayed in Figure 11.

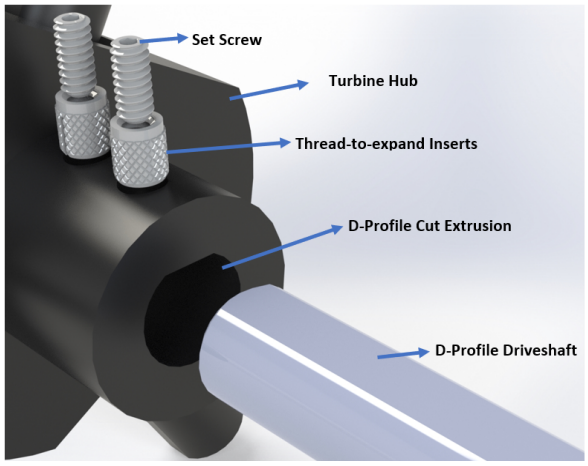

***Figure 10**: Exploded View of Driveshaft Mounting*

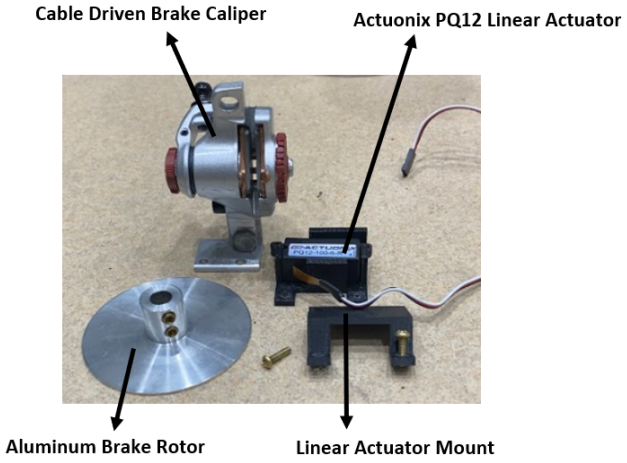

***Figure 11**: Emergency Brake Components*

2.2 Passive Yaw System

A passive yaw system was designed to continuously position the turbine upwind. It consists of two thrust bearings to support axial loads, and two ball bearings to support radial loads introduced to the system. These bearings translate the force from the changing wind direction that is captured by the tail fin, and rotates the nacelle around the tower's axis. A lock collar is used to secure the yaw system at the top of the turbine's tower, all enclosed by a 3D printed housing. This enclosure also provides a point of connection for the nacelle to the tower.

The tail fin is designed to remain parallel with the incoming wind direction. It was laser cut from a lightweight and durable recycled ⅛ inch acrylic sheet. Along with positioning the turbine into the incoming wind direction, the passive yaw system decreases structural load on the turbine tower by absorbing yaw moments that act on the turbine from the changing wind direction. Exploded views of both the yaw system's bearing configuration and tail fin mounting design are provided in Figures 12 and 13.

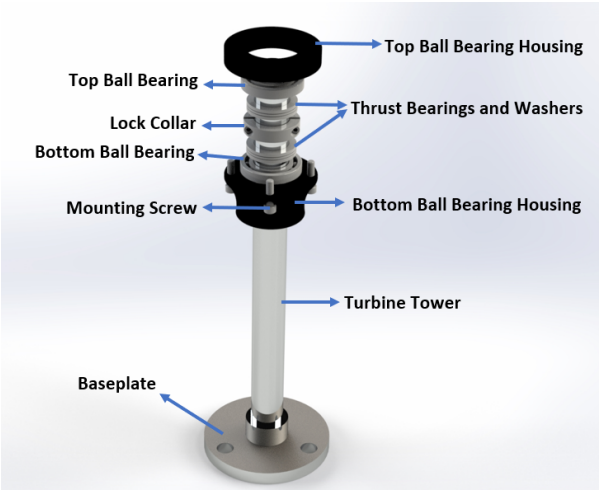

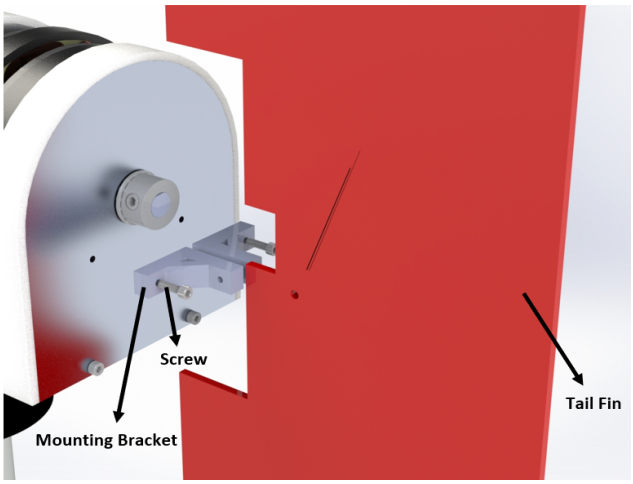

***Figures 12 & 13**: Exploded Views of Passive Yaw System*

2.3 Design Testing and Performance

To ensure the structural integrity of the wind turbine's mechanical and structural design, SolidWorks simulation studies were performed to analyze how the turbine's baseplate, tower, passive yaw system, and as well nacelle will react during both parked and operational conditions at 22 m/s wind speeds, as shown in Figure 14. For each scenario, the wind speed was converted into a wind load using the $\frac{1}{2}\rho u^2 A$ relation, where ρ is the air's density, u is the wind speed, and A is the either the frontal area or or blade swept area. Operating conditions were simulated based on the blade's swept area, whereas the parked conditions were based on the frontal area of the turbine. Higher structural loads were observed during operational conditions with a design safety factor of 3.9, whereas parked conditions yielded a safety factor of 9.7.

With respect to CWC's durability and power performance tasks, the passive yaw system needed to prove its functionality during various wind conditions over a wind speed interval of 5 m/s to 13 m/s. Through wind tunnel testing, the turbine's passive yaw system reacted to wind speeds as low as 3.5 m/s and allowed for proper alignment during cut-in tasks.. During physical testing and analysis, the weakest point in the design was found to be the turbine hub. At high torque loads the hub is at risk of slipping around the driveshaft. Despite the d-shape profile of the mounting design, the hub's ABS plastic material sacrifices durability at high wind speeds, specifically during parked conditions. The set screws, however, have proven to help the turbine withstand continuous wind tunnel testing without any signs of turbine hub slippage.

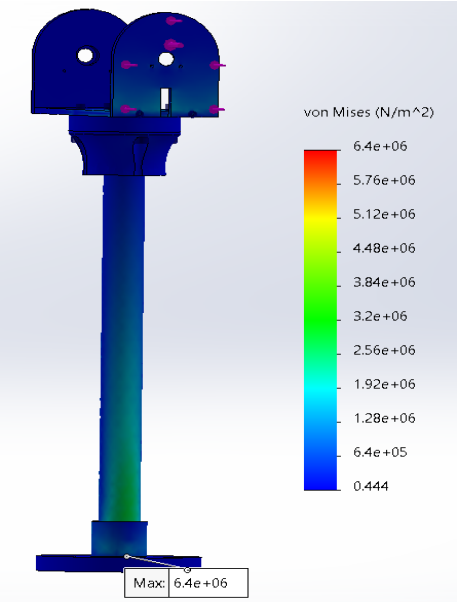

***Figure 14**: Turbine Structural Analysis*

3. Generator Design

During the conceptual phase of design, the team elected to design and fabricate a three phase, axial flux permanent magnet generator (AFPMG) because it allowed for optimization of power production when matched with the selected blade design. Although off the shelf motors were considered, an AFPM generator was chosen due to ease of fabrication and customization. This allowed the team to modify the generator voltage output range and efficiency by changing the coil winding density and air gap. Such design flexibility allowed the team to match the generator torque and power output characteristics to the chosen rotor blade and electronics design. The generator was the first component manufactured by the team because it represents the critical interaction point between the mechanical and electrical subsystems. All subsequent electronics tests with the system utilized this generator. The size of the generator also influenced all other component dimensions included in the nacelle.

3.1 Generator and Rotor Pairing

A Matlab model developed by prior JMU competition teams to predict power production of the generator based on the selected stator parameters was used to inform the final design. Torque vs. rotational speed simulations from QBlade were imported into a Matlab simulation that predicts the electrical and mechanical properties of a given AFPM configuration. Steady state operating speeds of the rotor and generator under different electrical loads are estimated through torque balance. Using this simulation, maximum power operating points and associated generator voltage, rotational speed, and resistive loading at each wind speed were estimated. Various generator stator designs were evaluated with different rotor blade design simulations to identify combinations that maximized scoring potential in the power curve task. Each stator design represented an alternate combination of selected stator parameters (i.e. wire gauge, coil turns, magnetic air gap, etc.). Using the information derived from these simulations, a 225 turn, 28 gauge magnet wire coil was selected as the optimal stator design that provides maximum power and competition scoring potential with the TSR 3.0 blade design while producing a rectified voltage below the 60 V input limits of the selected power conversion electronics. With this configuration, a maximum power production of 37.4 W at 11m/s was expected, along with a potential score of 49 for the power-curve task, as shown in Table 3 and Figure 15. At this wind speed and power production at the load, the selected generator design is expected to produce approximately 55 V at 0.8 A. With the selected

coil configuration, the total phase resistance through six coils is expected, and confirmed through measurement of the constructed generator, to be 20Ω. Therefore, the generator is expected to dissipate approximately 12.8W, representing a mechanical to electrical conversion efficiency of approximately 75%. However, as noted from testing, higher operating speeds resulted in a higher operating operating voltage, lower current, and increased generator efficiency.

Table 3: *Generator Design Comparison*

Design	Gauge	Number of Turns Per Coil	TSR	Projected Score
Alternate 1	28	200	3.0	48.82
Alternate 2	28	250	3.0	48.23
Selected Design	*28*	*225*	*3.0*	*49.69*
Alternate 3	26	250	3.0	46.11
Alternate 4	26	175	2.75	49.31

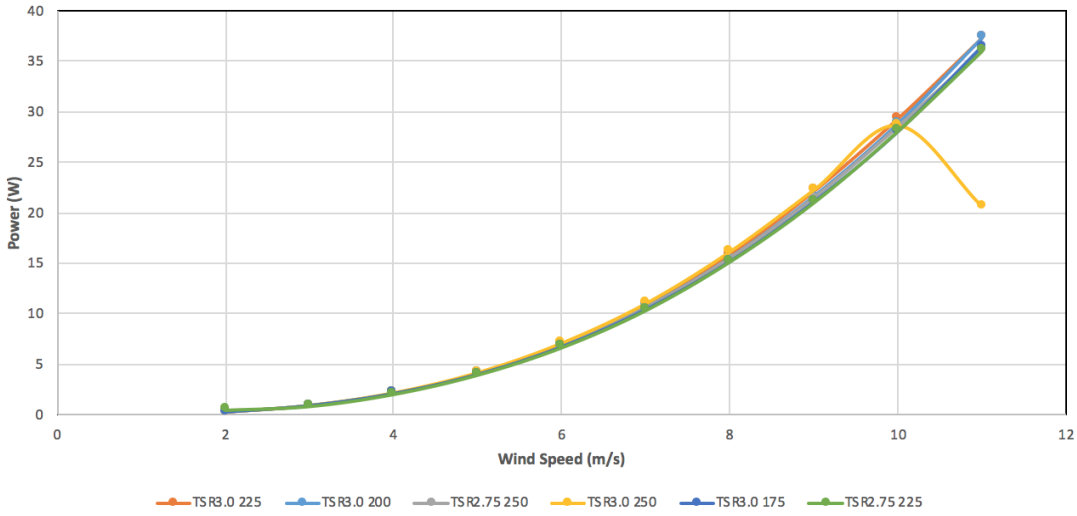

Figure 15: 28-Gauge Generator Performance Comparison

3.2 Fabrication

Each of the two generator rotors consists of an annular shaped 416 stainless steel plate with twelve 1 in. x 0.25 in. x 0.25 in. N52 neodymium magnets, arranged in alternating polarities, affixed to one side. The magnetic 416 stainless steel plate provides a low magnetic resistance to close the magnetic circuit and strengthen the magnetic flux through the stator air gap. The team utilized JMU's Fabrication Studio to 3D print housing which affixes the plate to the rotary shaft and serves as a guide for magnet positioning. Both rotor assemblies were then secured to the driveshaft using a set screw. An aluminum spacer was placed between the two magnetic rotors in order to obtain a tight magnetic air gap of 1 cm. The stator was composed of nine wire coils, with three sets of three coils each soldered together in series to form a phase. The phases were connected in a Wye configuration. The hand-wound 28-gauge, 225 turn magnet wire coils were inserted into a laser-cut mold and filled with epoxy resin to solidify the stator's shape. Each generator component is pictured below in Figure 16 , along with an exploded view model of the generator configuration in Figure 17.

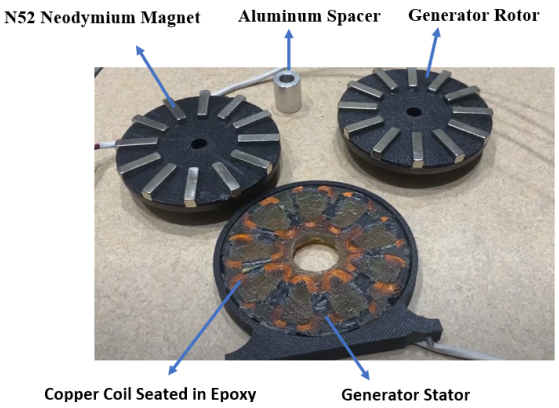

***Figure 16**: Generator Components*

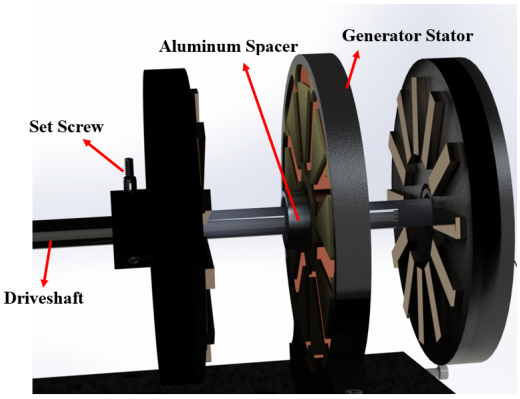

***Figure 17**: Generator Exploded View*

4. Electronics and Controls

The electrical system is designed to safely and efficiently supply maximum power produced by the turbine to the load. Figure 18 presents a simplified schematic of the entire prototype turbine electronics system. Three phase AC power is produced by the AFPMG and rectified to a DC output. The unregulated DC power is then measured by a current and voltage (I-V) sensor before being regulated to 12 V DC by a wide range input buck-boost converter. Additional buck converters are used to convert 12V into 6V and 7V required for actuators and sensors within the system. The electronic load is a controlled current sink and power resistor. The power switch and load side motherboard are continuously powered by a 120 VAC to 12 VDC converter that is plugged into a wall outlet. The power switch allows this 12V supply to be directed to the turbine through the PCC as required for restart control actions, such as restarting the brake and monitoring sensor outputs when the turbine is not producing sufficient power.

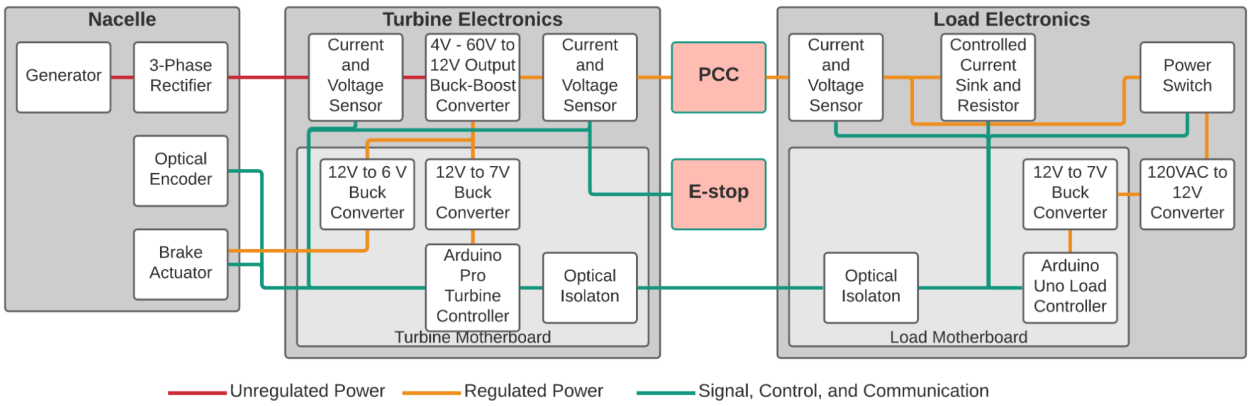

***Figure 18**: Electrical System Line Diagram*

To avoid challenges faced by prior teams with inconsistent electrical connections requiring frequent troubleshooting, all subcircuits in the electrical system were designed as custom PCBs, with the exception of the 12V buck-boost converter, which was purchased as a demo board, and the power switch, which was hand fabricated on a solderable prototyping board. All custom PCBs are interconnected using VH series JST keyed connectors or male pin headers combined with commercially available wires and cables. All external power connections use 15A Anderson Powerpole connectors while external data and communication connections are terminated with screw locking circular connectors. The turbine side and

load side electronics, and interconnections can be seen housed in their respective NEMA enclosures in Figure 19 below.

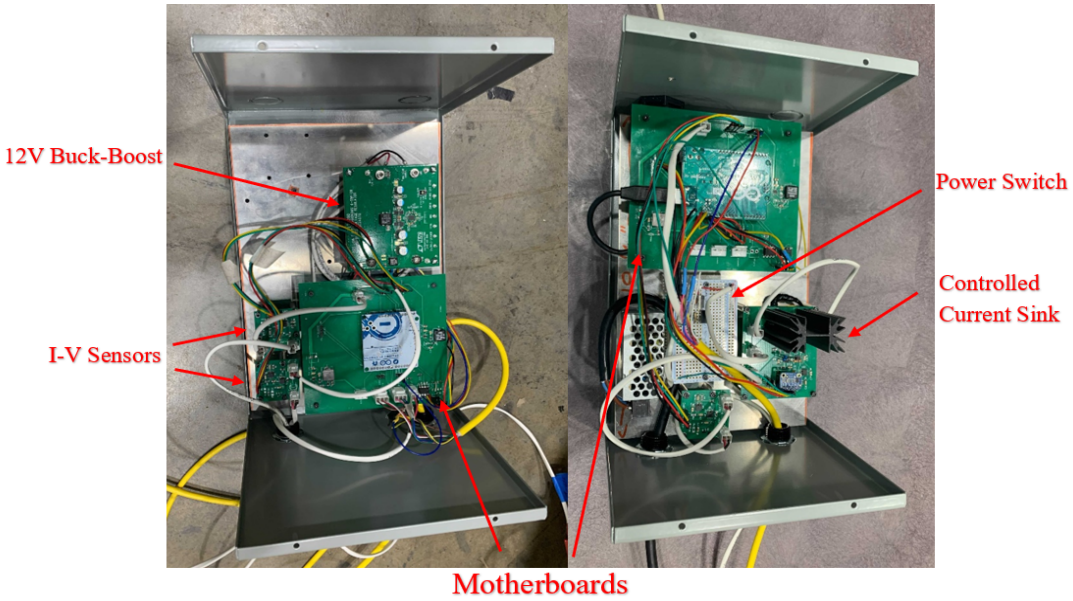

***Figure 19**: Turbine Side and Load Side Electronics Within NEMA Enclosures*

4.1 Rectification

The three phase AC output of the AFPM generator required rectification to DC. A MOSFET based ideal diode rectifier specified by the 2020 team and a Schottky diode rectifier were considered for this function. Although less efficient, a Schottky diode rectifier was selected due to ease of manufacturing, reliability, and component availability. Six 60V, 5A Schottky diodes, having a forward voltage of 0.52 V, were arranged on a custom designed circuit board in a full wave rectification configuration. At a wind speed of 11m/s, the generator is expected to produce a current of approximately 0.8 A, resulting in 0.83 W of dissipation by the rectifier.

4.2 Power Management and Energy Storage

The unregulated and rectified output of the rectifier is passed to a buck-boost converter, which regulates a 4 - 60 V input to a regulated 12 V output. This regulated 12 V is distributed to the system to power sensors, actuators, and the load. The wide range buck-boost converter was purchased off-the-shelf as a 12 V 4 A demonstration board using the LT8390 switching controller. Prior JMU teams connected the rectified generator output directly to the load. Implementing this buck-boost converter allows the generator to run at higher rotational speeds and output voltages without exceeding 48 V at the point of common coupling (PCC). This also allowed the team to use a higher TSR blade design and develop a more efficient generator stator. To meet the power requirements for the control electronics, two additional switching regulators based on the TPS56339 buck controller were incorporated into the custom designed motherboard to supply 6 V to the linear actuators and 7 V to the microcontrollers. Due to the presence of a linear regulator on the Arduino microcontroller boards, they may be supplied 7-12 V. Supplying 7 V to the microcontroller board reduces power loss in the linear regulator while still providing rejection of high frequency switching noise.

Energy storage on the turbine side electrical system consists of 42 capacitors and 4 inductors on the buck-boost converter, generator and load I-V sensors, and motherboard. The inductors range from 1.5 µH to 16 µH and capacitors range from 10 pF to 120 µF. The total energy storage capacity on the turbine side is 0.352 J, well below competition requirements of <10 J of combined energy storage.

4.3 Sensors

Three custom designed current and voltage (I-V) sensors were integrated into different points of the system's power path. These custom designed PCBs allowed configuration of voltage dividers and shunt current amplifiers to condition outputs for compatibility with the microcontrollers' 0-5 V analog to digital converter input range.

A U.S. Digital E5 optical encoder with a 100 count per revolution optical interrupter disk was selected to monitor the rotational speed of the drivetrain. Square wave pulse durations of the optical encoder output are measured by the microcontroller and used to estimate the rotational speed. Given the timing resolution of the Arduino microcontroller, this configuration allows for rotational speed measurements in excess of 10,000 RPM, well above the expected operating speed.

4.4 Load Configuration

The load system, represented schematically in Figure 20, is an analog controlled current sink with a 2.7 Ω resistor. The load system consists of an error amplifier with two inputs; a digital-to-analog signal commanded by the Arduino and the output of an instrumentation amplifier used to measure the potential difference across a 5 mΩ shunt resistor. The output of the error amplifier controls the gate voltage of an N-channel MOSFET to make the difference between the two inputs as close to zero as possible. This makes the current measured through the MOSFET and power resistor match the current command sent from the Arduino. A heat sink is used on the MOSFET because a temperature rise of about 30℃ is expected when it is acting as a resistor. The power resistor used as the load is rated for 100 W with high current handling and no current derating.

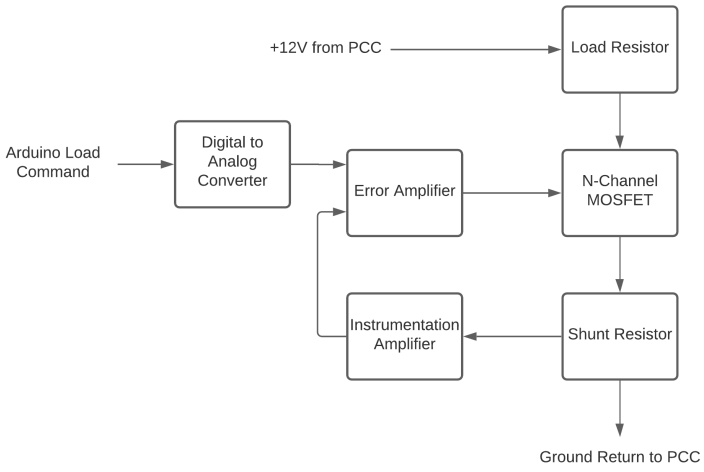

***Figure 20**: Line Diagram of Analog Controlled Load System*

An analog controlled load system was selected over a PWM controlled approach used by prior JMU teams because of the increased current control resolution of 1 mA. Further, removal of high frequency switching reduces noise and enhances power quality and stability.

4.5 Controls

Entire system control is achieved with two Arduino microcontrollers. An Arduino Uno on the load side, which is always powered, acts as the primary system controller. An Arduino Pro on the turbine side monitors generator outputs, rotational speed, the E-stop condition, and sends control signals to the

brake. The two controllers exchange information and commands via an 38,400 baud serial line that is optically isolated with two HCPL 2200 ICs. These serial communications may also be monitored using a USB connection on the load enclosure.

Figure 21 summarizes the primary control decisions and operational states for the system. For every cycle of the control loop, the main controller first verifies if communications have been received from the turbine. A lack of communication indicates that the turbine controller is not powered, due to low wind speeds, a parked condition, or a communication cable disconnection. When these conditions are observed, the controller provides power to the turbine from the load and commands the turbine controller to release or open the brake.

When communications are received, the controller primarily determines the operational state based upon the measured rotational speed and adjusts the load current and brake setting commands accordingly. At low wind speeds and measured rotational speeds, the load remains as an open circuit, allowing all power generated to be consumed to power the turbine electronics. Once a sufficient rotational speed is observed, the controller slowly increases the load current setting according to a linear progression with increasing speed. Above a threshold of 700 RPM, which corresponds to an approximate wind speed of 4 m/s, the controller enters a maximum power point tracking state.

Adjustment of the load for maximum power is achieved by monitoring the generator power produced and comparing the expected rotational speed to the observed rotational speed. The current command to the load is adjusted in proportion to the difference between the observed and expected rotational speed. That is, if the observed rotational speed is higher than the expected speed based on the generator power output, the load resistance is decreased to promote slowing of the rotor and an increase in power dissipation by the load. Through multiple trials and calibration runs, the team developed a reliable rotational speed vs. generator power function that is employed by the microcontroller. However, due to differences in the JMU wind tunnel and the competition tunnel, a verification of this calibration may be required.

If the rotational speed increases beyond a threshold corresponding to the desired rated power, a second algorithm modulates the brake position in proportion to the magnitude of the deviation from this setpoint to slow the rotor and reduce power production. This threshold can easily be adjusted in code. Because the JMU tunnel was capable of reaching speeds of 10 m/s in ideal conditions, this rated power threshold was set at a rotational speed corresponding to 8.5 m/s conditions to test this control feature. However, in the CWC tunnels, this threshold can be adjusted quickly.

Finally, the state control algorithm checks for emergency conditions, which supersede all prior identified states. The manual E-stop condition is identified by a change in the button state. The PCC power disconnect condition is identified by a difference between the turbine output voltage and the load input voltage. Once identified, both states command the brake to engage fully to stop the rotor.

Practice tests will be used to generate and confirm calibrations in the competition wind tunnel. A checklist has been established to ensure proper programming of variables in the microcontrollers and electrical connections are established prior to installation in the testing tunnel. Once installed for testing, the load will be powered, it will be verified that the brake has been removed and that communications are occuring between load and turbine. Once verified, the power will be removed to allow judges to confirm that there is no energy transfer through PCC. The load will again be powered to start the testing sequence.

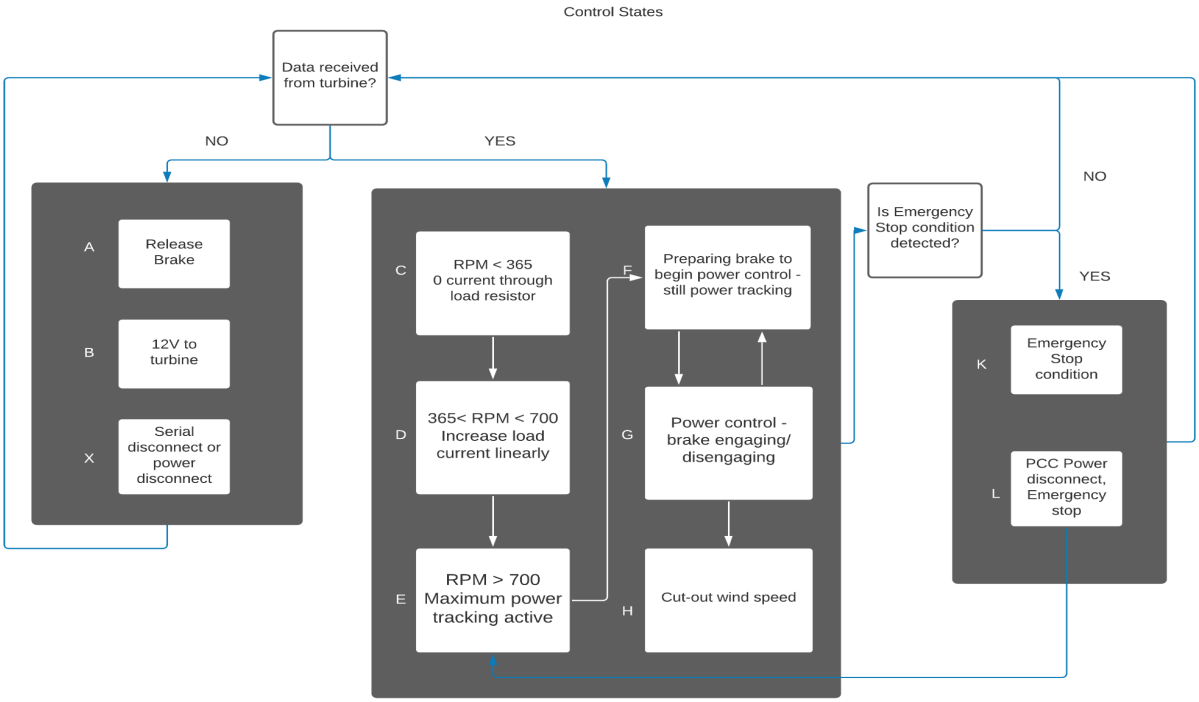

***Figure 21**: Control States Diagram*

5. New for 2021

JMU has regularly participated in the CWC since 2018. This history of participation has created a steady pipeline of knowledge transfer and allowed subsequent teams to build upon prior experiences. However, each year, the prototype development team thoroughly reviews prior designs and establishes their own approach. As a result, the 2021 JMU prototype design differs in many ways from that of the 2020 competition team's design. The challenges faced, decisions made, and feedback received during the 2020 competition influenced this year's 2021 turbine design. The following sections briefly describe design decision changes and similarities to the 2020 JMU CWC design.

5.1 Blade Design

JMU's 2021 team utilized the same blade design software and resources (airfoiltools.com, QBlade, SolidWorks) as the JMU 2020 team. The major difference in the blade design was the selection of a modified airfoil profile and design TSR. The 2021 team incorporated a blend of two airfoils (Wortmann FX 60-126 & SG6043) with similar angles of attack to optimize c_l/c_d and increase power production. The 2021 team also changed the blade and hub connection design by 3D printing a hollow blade base with two holes that will slide over the hub connection point and be secured by two machine screws. Although ultimately the team elected to use the same blade material (Onyx) as the 2020 team, more detailed experimentation and analysis of the material properties and characteristics were explored by the 2021 team.

5.2 Mechanical and Structural Design

JMU's 2020 design emphasized placement of all electronics inside the nacelle to minimize connection points and simplify turbine installation. Consequently, the nacelle was lengthened. To remain

within dimensional requirements, the 2020 team used a pair of parallel yaw fins. Due to COVID-19, the team was unable to test the reactiveness of the passive yaw system. However, considering that the tail design had a small surface area, the ability for the passive yaw system to position the turbine upwind at low wind speeds was of concern. Therefore the 2021 team reduced component placement in the nacelle This allowed for the design of a smaller nacelle and the mounting of a single, larger surface area tail fin to promote yaw under low wind conditions and increase yaw stability.

A few design aspects for this year's 2021 turbine prototype do reflect the previous design. The bearing configuration from last year's passive yaw system is very similar to this year's design given the need to select bearings that can support axial and radial loads introduced to the turbine system. JMU's 2021 passive yaw system design also utilizes the bearing housings as a point of connection for the nacelle to the turbine tower. A fixed pitch design was again selected for the 2021 competition to ensure simplicity and ease of manufacturing and assembly. Although the team carried out design efforts for an active pitch system, time, fabrication, and testing constraints resulting from COVID-19 resulted in the decision to forgo its implementation.

5.3 Generator Design

The overall generator design remained consistent with the 2020 team. The analysis and justification behind the JMU 2020 team's decision to select an axial flux permanent magnet generator design was elaborate and greatly influenced the 2021 team's decisions. The 2021 team utilized the extensive Excel and Matlab models developed by the prior team to guide the generator stator design process. However, specific parameters such as the wire gauge and number of turns in each coil were modified to complement blade and turbine system design decisions. The 2020 team designed a stator with 9 coils, each 300 turns of 28-gauge wire. This year, the generator was designed with 9 coils, each 225 turns of 28 gauge wire. The differences in this year's generator can be attributed to an increased tip speed ratio of 3.0 (vs. 2.0 prior) and the inclusion of a wide input buck-boost converter.

5.4 Electronics

Many aspects and subcircuit designs of the electrical system are different from the 2020 design, as noted in Section 4. This year's team elected to use a Schottky diode full wave rectifier instead of an ideal diode rectifier for simplicity of design and manufacturing. The team also elected to regulate the generator voltage, allowing an increased design TSR and generator voltages exceeding the 48 V. This is different from the previous teams that directly connected the load to the unregulated power produced by the generator. An RPM sensor was selected for the main instrument to determine the current wind speed and control state of the turbine. The team elected to use the RPM sensor instead of a pitot tube like the JMU 2020 team because of the complexity and inconsistency last year's team experienced with the pitot tube. Finally, an analog controlled current sink for the load system was designed as opposed to a PWM controlled system because of increased power quality and resolution.

5.5 Controls

Changes in controls between the 2020 and 2021 are primarily related to implementation and testing of the turbine. The 2020 team was not able to fully fabricate the turbine due to COVID-19 and therefore could not test the design. The 2020 team also were planning to rely on wind speed measurements using a pitot tube for control. The 2021 team used a different approach of power tracking to determine control states for the turbine.

6. Results

Although in-person competition testing was halted, the team attempted to replicate competition testing conditions using available university resources. Most competition tests were able to be

successfully performed with the exception of tests requiring wind speeds greater than 9.3 m/s, due to limitations of the team's home-built wind tunnel. The team documented all testing data and determined an estimated score based on the CWC scoring scale included in the Rules and Requirements.

6.1 Safety Inspection

Dr. Keith Holland, the team's capstone advisor, role played as a competition official in order to closely simulate the full competition experience. Dr. Holland inspected the team's turbine ensuring that all items included in Appendix B of the 2021 Rules and Requirements document were satisfied prior to testing.

6.2 Cut-In Wind Speed

Sporadic power production was observed by the team at 3.5 m/s (not exceeding 5s) while reliable power production was observed at 3.7 m/s. Therefore, the turbine's cut-in wind speed is 3.7 m/s. Considering drivetrain friction, electrical load, and a 3.7 m/s cut-in wind speed, QBlade was used to estimate that the turbine demands 1.5 mN•m of torque at the driveshaft to begin producing power. A fixed-pitch design with a design TSR of 3.0 sacrifices cut-in performance at low wind speeds, due to the blade's smaller surface area.

6.3 Power Curve Performance

The turbine was placed through a range of wind speeds in order to determine its power curve. At each wind speed from 3.7-9.3 m/s the voltage, current, power output, and rotational speed were recorded. For wind speeds above 9.3 m/s power production was estimated by fitting a model to the power results obtained at all previous wind speeds. The standard wind power equation, $P = \frac{1}{2}\rho A C_p \eta u^3$, was used as the basis for the model. The air density (ρ), based on barometric pressure, temperature, and humidity on testing day was 1.228 kg/m^3. The rotor COP (C_p) was estimated from Qblade simulations to be 0.37. A least squares fit was then used to determine an electrical conversion efficiency (η) of 0.83. This estimate was deemed reasonable when considering the combination of the advertised buck-boost converter efficiency of 95% and the expected generator efficiency of approximately 85%. Table 4 compares measured results to those predicted from design simulations. The turbine produced 22.21 W at the maximum tested wind speed of 9 m/s which very closely resembled the predicted power output of 22.17 W. Over a tested wind speed range of 5-9 m/s the greatest deviation between measured and simulated power was 1.07 W at 5 m/s.

***Table 4**: Measured and Simulated Power Production Comparison*

Wind Speed	**5 m/s**	**6 m/s**	**7 m/s**	**8 m/s**	**9 m/s**
Measured	3.05 W	6.31 W	10.29 W	15.11 W	22.21 W
Simulated	4.12 W	6.99 W	10.85 W	15.88 W	22.17 W

Additionally, the team observed a much higher measured tip speed ratio than predicted by simulation, shown in Table 5. The blades were designed for optimal power production at a TSR of 3. Theoretically, at 9 m/s with a TSR of 3, the blade tip velocity is 27 m/s which translates to an expected RPM of 1146. However, physical testing showed that maximum power output at 9m/s was obtained at 1860 RPM. At 1860 RPM the blade tip travels 43.6 m/s which indicates a realized TSR of 4.86. The difference in expected and realized TSR is most likely due to a greater average Reynolds number across the blade due to increasing wind speeds and blade velocity. The blades were modeled in QBlade at a

constant Reynolds number of 50,000; however, in real conditions the blades experienced a greater actual Reynolds number which increased lift and led to higher torque and operating speeds.

***Table 5**: Comparison of Measured and Predicted RPM and TSR*

Wind Speed	**5 m/s**	**6 m/s**	**7 m/s**	**8 m/s**	**9 m/s**
Measured	900 RPM TSR = 4.24	1160 RPM TSR = 4.55	1380 RPM TSR = 4.64	1610 RPM TSR = 4.74	1860 RPM TSR =4.86
Predicted	636.6 RPM TSR = 3.0	763.8 RPM TSR = 3.0	891 RPM TSR = 3.0	1018.8 RPM TSR = 3.0	1145.4 RPM TSR = 3.0

6.4 Control of Rated Power and Speed

Due to the limitations of our team's home-built wind tunnel, control of rated power was tested for wind speeds of 8.5m/s - 9m/s. The control of rated power and speed was achieved using the brake system to modulate the rotational speed of the rotor to maintain a set value of 1800 RPM, determined through testing trials for 8.5 - 9m/s wind speeds. Figures 23 and 24 present time series plots of the control of rated power and speed tests. Note the oscillation in rotational speed due to brake engaging and releasing the brake rotor.

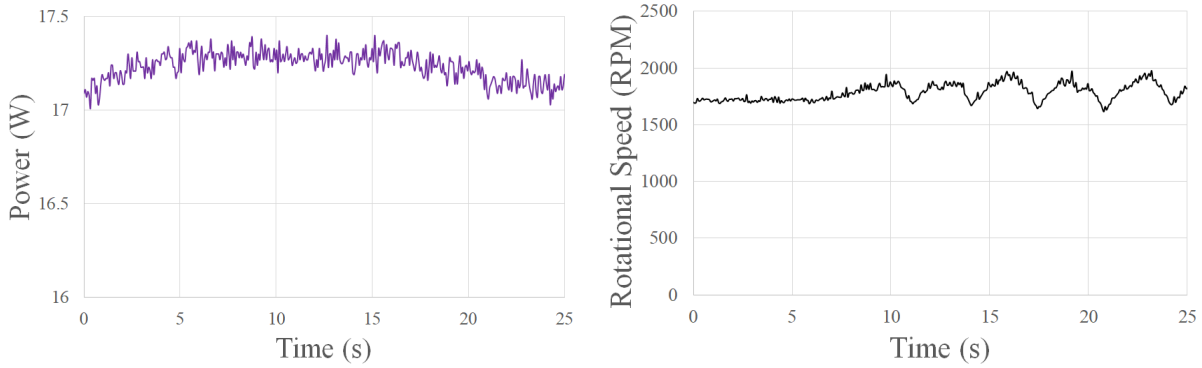

Figure 23 & 24: *Control Power Production and RPM Reading*

6.5 Safety Task

The turbine was run through a full safety test by demonstrating both E-stop and load disconnect shutdowns. The turbine was able to successfully come to a complete stop when the E-stop switch was initiated as well as when the load was disconnected from the circuit. Following each shutdown condition, the turbine was able to successfully restart and return to a power producing state.

7. Recommendations for the JMU CWC 2022 Team

JMU Engineering has a long history of participation in the Collegiate Wind Competition. Due to this, an extensive pipeline of information has been generated which is passed down to each year's rising competition team. This year, through fabrication and testing, our turbine prototype team discovered numerous ways to improve the performance of the wind turbine. The 2021 team's designed turbine begins to produce power at wind speeds as low as 3.5 m/s. In order to improve the cut-in wind speed it is suggested that the JMU 2022 turbine prototype team incorporate an active pitching system in the rotor design. By including an active pitching system in the design, the team will be able to avoid the inevitable tradeoff between torque produced at low wind speeds and efficient power extraction over a range of higher wind speeds. The active pitching system will allow the blades to be designed with a higher tip

speed ratio while still increasing torque at low wind speeds by pitching the blades towards the apparent wind. This will help lower the cut-in wind speed for the turbine design. There was a lot of progress made by this year's 2021 team on the mechanical design of the active pitch system, however, due to lab and time limitations the team shifted focus on completing the turbine prototype using a fixed-pitch design. To account for a higher realized TSR the team suggests that future teams include the impact of an increasing Reynolds number into blade performance models to more accurately predict operational RPM. A more accurate prediction of turbine operating speeds would allow teams to increase the generator efficiency by designing the generator for reduced resistance and power loss.

Considering turbine safety and durability, future CWC teams should manufacture all rotary components such as the turbine rotor hub and generator rotors from a non-magnetic, metallic material such as aluminum instead of 3D printed ABS plastic. This will eliminate the need for thread-to-expand inserts for any fastener such as set screws. Furthermore, thread-to-expand inserts are prone to cracking the 3D printed material which may lead to turbine failure. JMU's CNC machine is a great resource for manufacturing any component that may have a more complex geometry, such as a turbine rotor hub. To assist the turbine's controls, a pitot tube design is a great way to measure wind speed. However, due to multiple variables, lots of testing should be done to determine the accuracy of such measurement. This will give the team lots of room to test other control methods for the load and possibly achieve higher power output from the generator due to having a precise reading for the wind speed. It is important to note that integrating the pitot tube with the driveshaft will create complexity in the design. The pitot tube will need to remain stationary while the drivetrain components rotate around it. This may be achieved with a set of small ball bearings in which their inner race holds the pitot tube stationary, while the bearing's outer race allows for the driveshaft to rotate independently.

8. Conclusions

James Madison University's 2021 CWC Turbine Design Team focused efforts on simplicity when researching, designing, and fabricating a small-scale wind turbine for times of high uncertainty. With respect to the competition's rules and requirements, design efforts were set to increase energy capture, improve safety and control, enhance durability, and ensure ease of use of the turbine design. The team's fixed-pitch, direct drive, horizontal axis wind turbine design was successfully fabricated and tested which offered a learning experience that projected the interdependence of a wind turbine system. Incorporating a passive yaw system helped ensure energy captured was maximized, whereas a direct drive drivetrain helped reduce friction within the turbine system to assist with the cut-in wind speed task given the high TSR blade design. It was key to design the yaw system ensuring the turbine was reactive to low wind speeds and stable at high wind speeds, which were both influenced by the tail fin's surface area and friction within the yaw system's ball bearings. Developing code for the control system involved numerous amounts of trial and error. Ensuring the received data was accurate required calibration of the optical encoder and I-V sensors. Developing the control state of maximum power generation was the most complex portion of control due to the sensitivity of the turbine on load values, which would cause the rotor speed to rapidly increase or slow down to a near halt. Compromise, patience, and persistence are the keys to success in a project such as this.

The learning experience for JMU's 2021 CWC turbine development team went beyond the technical design of the prototype wind turbine. Opportunities to gain an understanding of project development and the business side of the wind industry were offered through two classes covering project management and wind farm modeling. Information from these courses helped build an understanding of the process used to formulate a wind farm siting plan. This opportunity was unique given the continuous interactions that the team had with the project development team where we learned how to bridge the communication gap between those working on the same project from different disciplines.

The James Madison University 2021 CWC Turbine Design Team would like to thank the DOE and CWC organizers for this opportunity. We appreciate your efforts to provide a valuable learning experience despite the barriers presented by COVID-19.

References

[1] Marten, et al. *QBlade: An open source tool for design and simulation of horizontal and vertical axis wind turbines.* International Journal of Emerging Technologies and Advanced Engineering, 3 (3), 2013. https://ijetae.com/files/Conference%20ICERTSD-2013/IJETAE_ICERTSD_0213_41.pdf

[2] *Onyx - Composite 3D Printing Material.* Markforged. Retrieved 2021, https://markforged.com/materials/plastics/onyx